

High Performance Operation of a Direct-Current and Superconducting Radio-Frequency Combined Photocathode Gun

H. Jia*, T. Li*, T. Wang, Y. Zhao, X. Zhang, H. Xu, Z. Liu, J. Liu, L. Lin,

H. Xie, L. Feng, F. Wang, F. Zhu, J. Hao, S. Quan, K. Liu, and S. Huang[†]

*State Key Laboratory of Nuclear Physics and Technology and Institute of Heavy Ion Physics,
School of Physics, Peking University, Beijing 100871, China*

Superconducting radio-frequency (SRF) guns are promising candidates to deliver high brightness continuous-wave (CW) electron beams for new generations of coherent linac light sources, ultrafast electron diffractions, MeV pulsed beam applications, etc. To solve the compatibility problem of semiconductor photocathodes, a hybrid gun combining a direct-current gap and an SRF cavity has been developed. The gun, employing K_2CsSb photocathodes driven by a green laser, has been brought into stable CW operation with a dark current below 100 pA, delivering electron beams at an energy gain of 2.4 MeV, an electron bunch charge of 100 pC, and a repetition rate of 1 MHz. A normalized beam emittance of 0.54 mm-mrad has been achieved at the bunch charge of 100 pC and peak current of about 6 A. CW operation at 81.25 MHz repetition rate has also been tested with the maximum average beam current reaching 3 mA.

Photocathode guns are the most important high brightness electron sources [1, 2], whose technical advancement has greatly promoted the development and applications of electron accelerators, such as free-electron laser (FEL) [3–6], energy recovery linac (ERL) [7, 8], ultrafast electron diffraction [9], etc. The achievements made in these applications in turn have placed higher demands on photocathode guns [10, 11]. Especially, generating megahertz (MHz)-rate high brightness electron beams with low dark current becomes a hot topic during the past two decades [12].

To accelerate MHz-rate beams, continuous-wave (CW) operation of a radio-frequency (RF) cavity is needed, which adds great challenges for a normal conducting RF gun due to huge heat load and high dark current [12]. On the other hand, superconducting RF (SRF) guns are the natural candidate for CW RF operations due to the low power dissipation on the cavities [13–17]. However, outstanding challenges still remain, such as photocathode integration into the SRF structure, emittance compensation, etc. [11]

In this Letter, we report the latest breakthroughs achieved with a direct-current (DC) and SRF combined photocathode gun at Peking University. We will first present a brief overview of the design considerations and main features. Then we will show the commissioning results. Especially, we demonstrate the emittance compensation [18–20] and multipole magnetic field corrections [21, 22], which are crucial for achieving low beam emittance as required by CW X-ray FELs.

The concept of DC-SRF gun was originally proposed in 2001 to address the problem of compatibility between semiconductor photocathodes and SRF cavity [23]. It combines a pair of DC high voltage electrodes and a 1.3 GHz SRF cavity connected by a short drift tube (about

10 mm long), as shown in Fig. 1(a). The photocathode is located in the DC gap and therefore separated from the cavity. This design has a few advantages: 1) it allows to use a normal conducting photocathode in an SRF gun, and isolation with an RF choke filter [11] is not needed any more; 2) it avoids the potential contamination of SRF cavity from the semiconductor materials; 3) it greatly diminishes the dark current arising from the rim of photocathode plug or the cathode nose. The short distance between the DC gap and the cavity allows the required DC voltage to be a few tens to 100 kV, which puts less stringent requirements on high voltage components and makes the gun very compact. Besides, the DC-SRF hybrid structure provides an excellent vacuum environment for sensitive photocathodes, especially bi-alkali photocathodes which have significant quantum efficiency (QE) in green region of light spectrum. This helps greatly reduce the requirements on drive lasers for MHz-rate operation.

The development of DC-SRF gun has undergone three stages: the prototype for feasibility test [24, 25], the first generation (DC-SRF-I) achieving stable operation in pulse mode [26], and the second generation (DC-SRF-II) attaining low emittance CW operation. Here the DC-SRF-II gun represents a milestone. The operating voltage of the DC gap has been raised to 100 kV and the electric field at the photocathode surface is 6 MV/m accordingly. The SRF cavity, which has 1.5 cells, can be operated at a gradient (E_{acc}) of 14.5 MV/m in CW mode, corresponding to an on-axis peak electric field of 22.5 MV/m. For comparison, the DC-SRF-I gun could only be operated with a maximum DC voltage of 50 kV and a highest cavity gradient of 9 MV/m in pulse mode [27]. These significant advancements lay an important foundation for achieving low emittance beams.

As a substantial change to the previous version, the DC-SRF-II gun adopts K_2CsSb as photocathode material instead of Cs_2Te . The K_2CsSb photocathodes prepared for the gun have a QE above 5% at 515 nm [28],

* Contribute equally to this work.

[†] huangsl@pku.edu.cn

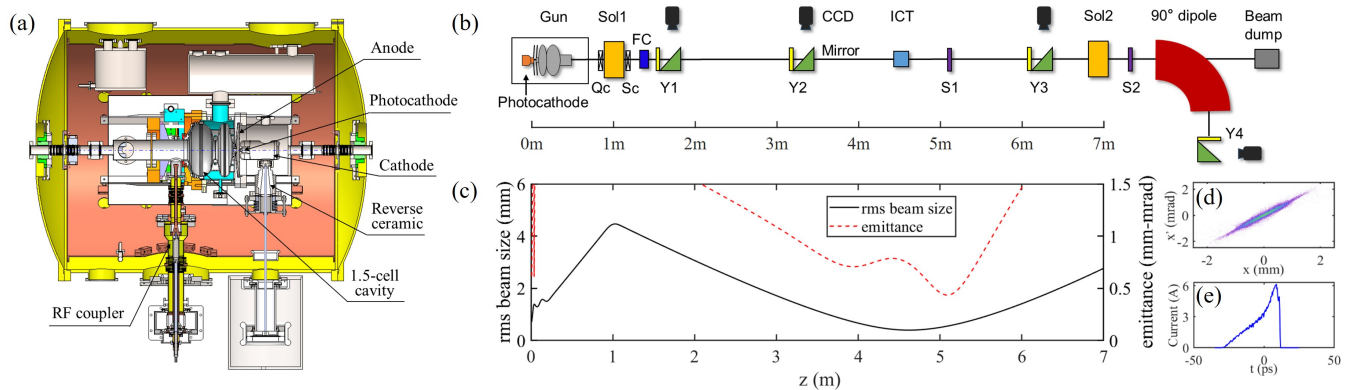


Figure 1. A sketch of the DC-SRF-II gun (a), the electron beam line (b), the simulated beam size and emittance along the beam line (c), and the phase space (d) and current profile (e) at S1. The beam line comprises two solenoid lenses (Sol1-Sol2), quadrupole coils (Qc), sextupole coils (Sc), a 90° dipole magnet, four pneumatic YAG screens (Y1-Y4), two motorized molybdenum plate with single slit (S1-S2), a Faraday cup (FC), an integrated current transformer (ICT), and a beam dump.

providing tremendous flexibility in the design of drive laser. For the DC-SRF-II gun, a drive laser based on an all-fiber master oscillator power amplifier has been developed [29], which can deliver CW laser pulses at 1 MHz or 81.25 MHz rate and provide pulse trains with flexible timing patterns for gun commissioning. More importantly, the drive laser can reliably operate at an average power up to 10 W. The sufficient margin for power loss allows the utilization of high-quality laser shaping, which is of essential importance for optimizing the low emittance electron beam. Besides, it is worth noting the K_2CsSb photocathodes are expected to have a lower intrinsic emittance compared to Cs_2Te photocathodes as widely used in normal conducting RF guns, which would also help reduce the beam emittance [30, 31].

The commissioning of the gun was started in 2021. As one of the major concerns for CW operation, the dark current from the gun, originating from the field emission on the inner surface of the DC gap and SRF cavity, has been carefully investigated. Experiments were first performed to evaluate the dark current from the DC gap under the same condition of CW operation while the drive laser was purposely blocked. In the measurement, the DC voltage was at 100 kV, while the cavity was operated with a lower gradient of 10 MV/m so as to mitigate its contribution. The field-emitted electrons, focused by a solenoid lens at the exit of the gun (Sol1), were collected by a Faraday cup (FC) as shown in Fig. 1(b), and the current was recorded by a picoammeter with a resolution of 0.1 pA. The solenoid strength was carefully scanned over a large range, while the readout of the picoammeter remained at zero, indicating the dark current from the DC gap was less than 0.1 pA.

The dark current investigation was then focused on the SRF cavity only. Fig. 2 shows a typical measurement of dark current as a function of the cavity gradient, where the DC voltage was zeroed and the cavity was operated in pulsed mode with a duty factor of 10% for safety considerations. The measurement results can be extrapolated to CW mode, since the dark current has a linear dependency on the RF duty factor (see Inset (a)). It can

be inferred that the dark current is below 100 pA when the cavity is operated in CW mode with a gradient up to 14 MV/m. An image of the field-emitted electrons is also shown in Fig. 2, for which the electrons were focused onto a YAG screen (Y1) right after the Faraday cup. The solenoid strength was close to that required to focus the photoelectrons from the gun, implying a similar electron energy, while the ring-shaped profile further suggests the electrons were emitted around the entrance iris of the cavity. It is worth noting there is a stronger emission region in the lower right of the dark current ring, indicating a defect area therein. However, this also means the dark current might be reduced through a careful processing of the cavity. Note this level of dark current (~ 100 pA) is about 4 orders lower than that in the current normal conducting CW guns such as the one at the LCLS-II (a few μA level) [32]. We believe such a low dark current will greatly reduce the operation challenges.

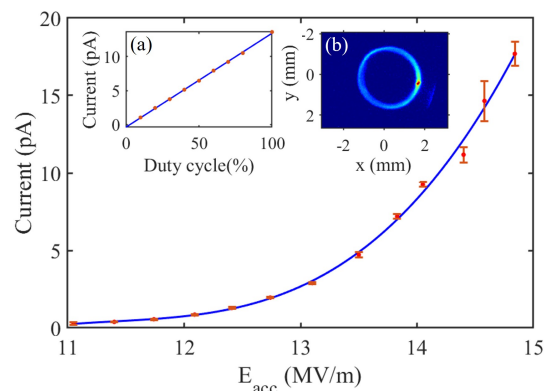


Figure 2. Dark current vs cavity gradient in pulsed mode with a duty factor of 10%. Inset (a) shows the dark current vs RF duty factor at the gradient of 12.3 MV/m; (b) shows an image of the field-emitted electrons.

The electron beam line illustrated in Fig. 1(b) was specially designed to demonstrate the feasibility of the DC-SRF-II gun as an electron source for CW XFELs. The Sol1 solenoid, whose center is at 1 m downstream the photocathode, is used for beam focusing and transverse emittance compensation. The emittance measure-

ment device (EMD), based on a single slit scanning method [33], comprises a motorized molybdenum plate with a $30\ \mu\text{m}$ wide vertical slit (S1) for beamlet sampling and a YAG screen (Y3), integrated with a 45° reflection mirror and a CCD camera, for electron divergence angle measurement. The EMD slit is located at 5.105 m downstream the photocathode, where the projected emittance at 100 pC bunch charge is expected to be well compensated according to simulation. It should be noted the electron beam from the gun has a rotationally symmetric distribution in the transverse directions, therefore only the horizontal EMD has been installed. The electron energy is measured with a dipole spectrometer, where a 90° dipole magnet with a bending radius of $R = 0.4\ \text{m}$ is employed, and the beam is first collimated by a $30\ \mu\text{m}$ wide slit (S2) and focused by a solenoid lens (Sol2) to improve the energy resolution.

Compared to pulsed photocathode RF guns, the DC-SRF-II gun has a lower electric field at the photocathode surface. To mitigate the space charge induced emittance growth, the photocathode drive laser should have a longer pulse duration and a larger transverse size. In such a case, the electron beam would have a large transverse size before being focused by the Sol1 solenoid, as can be seen in Fig. 1(c). This makes the electron beam transport very sensitive to multipole field errors, especially of the emittance compensation solenoid where the electron beam size is a few millimeters (root mean square, rms). To mitigate the impact of the undesirable quadrupole and sextupole field components, two sets of coils are installed around the Sol1 solenoid, as shown in Fig. 1(b). The one before the solenoid, Qc, comprises eight coils configured to produce quadrupole field rotatable around the axis, while the other one, Sc, comprises six coils mounted on a rotating frame to produce rotatable sextupole field.

Another measure to mitigate the impact of multipole field errors is beam based alignment. It was performed in two steps while operating the gun in pulsed mode with a bunch charge of 0.1 to 0.5 pC. For the first step, the fields of all the magnets before the Y1 screen were set to zero and the position of drive laser spot on the photocathode was adjusted till the central position of the beam on the screen would not change when altering the SRF cavity phase. This indicates the electron beam orbit is coincident with the axis of the cavity. For the second step, the Sol1 solenoid was turned on and its strength was scanned. When the beam orbit is off axis in the solenoid, the scanning would lead to a change of beam position on the Y1 screen. It traced out a curve while recorded by CCD camera, from which the alignment error was derived and the Sol1 solenoid was realigned accordingly.

The emittance optimization was focused on the high brightness operation mode at 100 pC bunch charge and 1 MHz rate. The DC voltage was at 100 kV and the cavity was operated with a gradient of about 14 MV/m. The photocathode drive laser had a longitudinally quasi-plateau distribution with a length of 34 ps and a rising/falling edge of 6 ps, which was achieved through pulse

stacking [29]. While in transverse plane, it had a truncated two-dimensional Gaussian distribution with the upper and lower limits at $\pm\sigma_0$, where σ_0 , the standard deviation of Gaussian function, was 1 mm. Simulation studies show the optimal normalized emittance could reach 0.44 mm-mrad at a kinetic energy of 2.43 MeV and a peak current of 6 A with proper compensation under the above conditions (see Fig. 1(c-e)). Note the emittance could be further improved by increasing the cavity gradient or optimizing the temporal profile of the drive laser including reducing the rising/falling edge. Our simulation study on a DC-SRF-II based 100 MeV injection line for CW XFELs has also demonstrated a normalized emittance below 0.4 mm-mrad and good longitudinal phase space performance under moderate operation conditions [34].

To characterize the CW performance of the gun, a dedicated beam diagnostics mode was designed, for which the 1 MHz photocathode drive laser was modulated to generate low duty cycle electron bunch trains while keeping all other parameters the same as CW operation. The optimization process started with a two-dimensional scanning of the cavity phase and solenoid strength to determine the optimal phase for minimum emittance, which was 0° (the on-crest acceleration phase) in the case reported herein. Then the acceleration phase was fixed at the optimal value and the electron beam phase space in the horizontal direction at different solenoid strengths was captured by the EMD with a small scanning step. To avoid the underestimation of emittance when excluding the invalid region of the captured images, two steps were taken to collect the data. First, the electron distributions along x (position) and x' (divergence angle) coordinates were both fitted to Gaussian functions with a standard deviation of σ_x and $\sigma_{x'}$, respectively, and the phase space area within $(-3\sigma_x, 3\sigma_x)$ and $(-3\sigma_{x'}, 3\sigma_{x'})$ were extracted. Second, the data points for 5% of the particles in the periphery region, which should contain some contribution from noise, was discarded. In this case, at least 95% of the particles were included in the calculation. From the electron phase space, the normalized emittance can be evaluated as $\epsilon_n = \gamma\beta\sqrt{\langle x^2\rangle\langle x'^2\rangle - \langle xx'\rangle^2}$, where β is the electron velocity scaled by the light speed in vacuum, γ is the Lorentz factor, while $\langle x^2\rangle$, $\langle x'^2\rangle$, and $\langle xx'\rangle$ denote the second-order moments of x and x' . A plot of the measured emittance is shown in Fig. 3, which arrives at its minimum of 0.73 mm-mrad at the solenoid strength of 552 Gs (blue curve without correction yet).

During the above experiments, a clear distortion of the electron distribution due to multipole magnetic field errors could be observed, as shown in Fig. 3. To quantify the effective multipole field components, the electron distribution was captured on the Y2 screen, where the electron beam still had a larger transverse size. The contour for the image was then extracted, as illustrated in Inset (a), from which the strength and angle of the effective quadrupole and sextupole fields were derived. For the optimal case presented in Fig. 3, the effective quadrupole

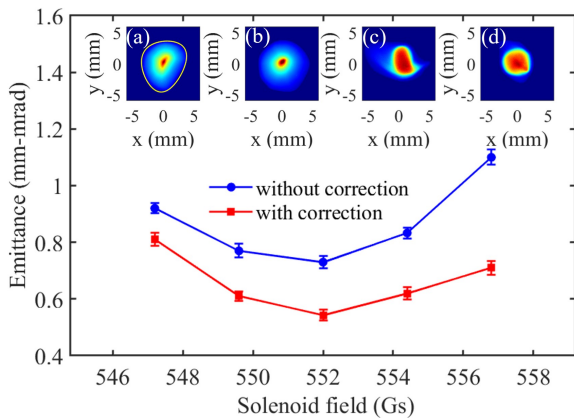


Figure 3. Normalized emittance vs compensation solenoid strength before and after multiple field correction. Insets (a)/(c) show the transverse beam images at Y2/Y3 before corrections, while (b)/(d) show the images after corrections.

component had an integrated field strength of 1.76 Gs and an orientation angle of 112° , while the effective sextupole component had an integrated field strength of 1.4 Gs/cm and an orientation angle of 31° . Subsequently, the quadrupole and sextupole correcting coils were set accordingly to cancel out the effect of multipole field errors. This led to a more regular and symmetric electron distribution shown in Insets (b) and (d). Such a correction was made at each instance in Fig. 3 and the emittance was reduced significantly. Especially, for the optimal case, a normalized emittance of 0.54 mm-mrad has been achieved, which is close to the simulation result.

Fig. 4(a) shows the horizontal phase space of the electron beam with multipole field corrections, from which the fractional normalized emittance ϵ_{nf} as a function of particle fraction ξ has been calculated, as plotted in Fig. 4(d). The core emittance and core fraction, defined according to [35], have also been derived, which are 0.28 mm-mrad and 70%, respectively, for this optimal case with 100 pC bunch charge. A summary of the parameters can be found in Tab. I.

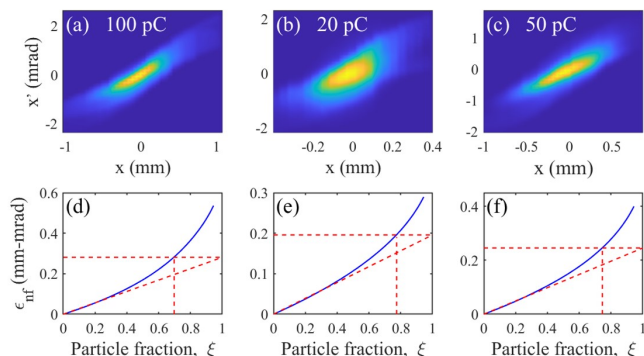


Figure 4. Electron beam phase space (a-c) and corresponding fractional normalized emittance vs particle fraction (d-f).

The emittance optimization was also performed at 50 pC and 20 pC bunch charges with the same drive laser temporal profile as the 100 pC case. The phase spaces with multipole field corrections are shown in Fig. 4, while the parameters are summarized in Tab. I.

Table I. Measured emittance and relevant parameters.

Parameters	100 pC	50 pC	20 pC	Units
SRF cavity gradient	14.4	14	14	MV/m
Drive laser size (σ_0)	1.0	1.0	0.8	mm
Electron beam energy	2.42	2.35	2.35	MeV
Normalized emittance	0.54	0.40	0.28	mm-mrad
Core emittance	0.28	0.25	0.19	mm-mrad
Core fraction	70%	75%	77%	

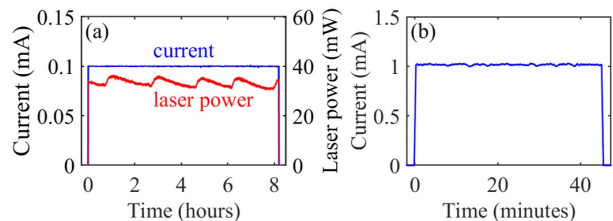


Figure 5. Average beam current during CW operation tests at 1 MHz (a) and 81.25 MHz (b). The photocathode drive laser power is also plotted in (a).

CW operations of the gun were mainly demonstrated at 1 MHz rate and 100 pC bunch charge. Fig. 5(a) shows the beam current monitoring results during a long-term run, which was recorded by the integrating current transformer (ICT) in Fig. 1(b). In the experiments, a beam current feedback based on photocathode drive laser attenuation was applied to maintain a constant current. The drive laser power is also plotted in Fig. 5(a), showing a cyclic change in a few hours' period. Such a phenomenon, only observed when the gun was operated in CW mode or high duty cycle quasi-CW mode, should be partially related to the local heating of the photocathode in its cryogenic environment, or the laser/mirror drifting at higher power. Although the mechanism for this variation needs to be further investigated, over one month's operation with a single photocathode in the gun at a QE of about 1% has already demonstrated the compatibility of the K_2CsSb photocathode and the gun.

Electron beam tests were carried out at 81.25 MHz rate, too. Fig. 5(b) shows the case at the kinetic energy of 1.7 MeV and average current of 1 mA. Short-term tests were also performed with a current up to 3 mA, while long-term operation at a higher current is expected in the future.

In conclusion, the DC-SRF-II gun has been brought into stable CW operation at 1 MHz rate, while the dark current is below 100 pA. A normalized beam emittance of 0.54 mm-mrad has been achieved at the bunch charge of 100 pC and peak current of 6 A, which meets the requirements of CW XFELs on electron guns. CW operation has also been tested with the maximum average beam current reaching 3 mA.

This work is supported by the National Key Research and Development Program of China (Grant No. 2016YFA0401904).

- [1] T. Rao and D. H. Dowell, “An engineering guide to photoinjectors,” (2014), arXiv:1403.7539 [physics.acc-ph].
- [2] F. Stephan and M. Krasilnikov, “High brightness photo injectors for brilliant light sources,” in *Synchrotron Light Sources and Free-Electron Lasers: Accelerator Physics, Instrumentation and Science Applications*, edited by E. Jaeschke, S. Khan, J. R. Schneider, and J. B. Hastings (Springer International Publishing, Cham, 2014) pp. 1–38.
- [3] P. Emma, R. Akre, J. Arthur, R. Bionta, C. Bostedt, J. Bozek, A. Brachmann, P. Bucksbaum, R. Coffee, F. J. Decker, Y. Ding, D. Dowell, S. Edstrom, A. Fisher, J. Frisch, S. Gilevich, J. Hastings, G. Hays, P. Hering, Z. Huang, R. Iverson, H. Loos, M. Messerschmidt, A. Miahnahri, S. Moeller, H. D. Nuhn, G. Pile, D. Ratner, J. Rzepiela, D. Schultz, T. Smith, P. Stefan, H. Tompkins, J. Turner, J. Welch, W. White, J. Wu, G. Yocky, and J. Galayda, *Nature Photonics* **4**, 641 (2010).
- [4] C. Bostedt, S. Boutet, D. M. Fritz, Z. Huang, H. J. Lee, H. T. Lemke, A. Robert, W. F. Schlotter, J. J. Turner, and G. J. Williams, *Rev. Mod. Phys.* **88**, 015007 (2016).
- [5] W. Decking, S. Abeghyan, P. Abramian, A. Abramsky, A. Aguirre, C. Albrecht, P. Alou, M. Altarelli, P. Altmann, K. Amyan, and et al., *Nature Photonics* **14**, 391 (2020).
- [6] E. Prat, R. Abela, M. Aiba, A. Alarcon, J. Alex, Y. Arbelo, C. Arrell, V. Arsov, C. Bacellar, C. Beard, P. Beaud, S. Bettoni, R. Biffiger, M. Bopp, H.-H. Braun, M. Calvi, A. Cassar, T. Celcer, M. Chergui, P. Chevtsov, C. Cirelli, A. Citterio, P. Craievich, M. C. Divall, A. Dax, M. Dehler, Y. Deng, A. Dietrich, P. Dijkstal, R. Dinapoli, S. Dordevic, S. Ebner, D. Engeler, C. Erny, V. Esposito, E. Ferrari, U. Flechsig, R. Follath, F. Frei, R. Ganter, T. Garvey, Z. Geng, A. Gobbo, C. Gough, A. Hauff, C. P. Hauri, N. Hiller, S. Hunziker, M. Huppert, G. Ingold, R. Ischebeck, M. Janousch, P. J. M. Johnson, S. L. Johnson, P. Juranić, M. Jurcevic, M. Kaiser, R. Kalt, B. Keil, D. Kiselev, C. Kittel, G. Knopp, W. Koprek, M. Laznovsky, H. T. Lemke, D. L. Sancho, F. Löhl, A. Malyzhenkov, G. F. Mancini, R. Mankowsky, F. Marcellini, G. Marinkovic, I. Martiel, F. Märki, C. J. Milne, A. Mozzanica, K. Nass, G. L. Orlandi, C. O. Loch, M. Paraliiev, B. Patterson, L. Patthey, B. Pedrini, M. Pedrozzi, C. Pradervand, P. Radi, J.-Y. Raguin, S. Redford, J. Rehanek, S. Reiche, L. Rivkin, A. Romann, L. Sala, M. Sander, T. Schietinger, T. Schilcher, V. Schlott, T. Schmidt, M. Seidel, M. Stadler, L. Stingelin, C. Svetina, D. M. Treyer, A. Trisorio, C. Vicario, D. Voulot, A. Wrulich, S. Zerdane, and E. Zimoch, *Nature Photonics* **14**, 748 (2020).
- [7] G. Neil, C. Behre, S. Benson, M. Bevins, G. Biallas, J. Boyce, J. Coleman, L. Dillon-Townes, D. Douglas, H. Dylla, R. Evans, A. Grippo, D. Gruber, J. Gubeli, D. Hardy, C. Hernandez-Garcia, K. Jordan, M. Kelley, L. Merminga, J. Mammosser, W. Moore, N. Nishimori, E. Pozdeyev, J. Preble, R. Rimmer, M. Shinn, T. Siggins, C. Tennant, R. Walker, G. Williams, and S. Zhang, *Nucl. Instrum. Methods Phys. Res., Sect. A* **557**, 9 (2006).
- [8] M. Akemoto, D. Arakawa, S. Asaoka, E. Cenni, M. Egi, K. Enami, K. Endo, S. Fukuda, T. Furuya, K. Haga, R. Hajima, K. Hara, K. Harada, T. Honda, Y. Honda, T. Honma, K. Hosoyama, E. Kako, H. Katagiri, H. Kawata, Y. Kobayashi, Y. Kojima, Y. Kondou, O. Tanaka, T. Kume, M. Kuriki, H. Matsumura, H. Matsushita, S. Michizono, T. Miura, T. Miyajima, S. Nagahashi, R. Nagai, H. Nakai, H. Nakajima, N. Nakamura, K. Nakanishi, K. Nigorikawa, N. Nishimori, T. Nogami, S. Noguchi, T. Obina, F. Qiu, H. Sagehashi, H. Sakai, S. Sakanaka, S. Sasaki, K. Satoh, M. Sawamura, M. Shimada, K. Shinoe, T. Shishido, M. Tadano, T. Takahashi, R. Takai, T. Takenaka, Y. Tanimoto, T. Uchiyama, A. Ueda, K. Umemori, K. Watanabe, and M. Yamamoto, *Nucl. Instrum. Methods Phys. Res., Sect. A* **877**, 197 (2018).
- [9] D. Filippetto, P. Musumeci, R. K. Li, B. J. Siwick, M. R. Otto, M. Centurion, and J. P. F. Nunes, *Rev. Mod. Phys.* **94**, 045004 (2022).
- [10] B. Dunham, J. Barley, A. Bartnik, I. Bazarov, L. Cultrera, J. Dobbins, G. Hoffstaetter, B. Johnson, R. Kaplan, S. Karkare, V. Kostroun, Y. Li, M. Liepe, X. Liu, F. Loehl, J. Maxson, P. Quigley, J. Reilly, D. Rice, D. Sabol, E. Smith, K. Smolenski, M. Tigner, V. Vesherevich, D. Widger, and Z. Zhao, *Applied Physics Letters* **102**, 034105 (2013).
- [11] R. Xiang, A. Arnold, and J. W. Lewellen, *Frontiers in Physics* **11** (2023), 10.3389/fphy.2023.1166179.
- [12] F. Zhou, C. Adolphsen, D. Dowell, and R. Xiang, *Frontiers in Physics* **11** (2023), 10.3389/fphy.2023.1150809.
- [13] I. Petrushina, V. N. Litvinenko, Y. Jing, J. Ma, I. Pinayev, K. Shih, G. Wang, Y. H. Wu, Z. Altinbas, J. C. Brutus, S. Belomestnykh, A. Di Lieto, P. Inacker, J. Jamilkowski, G. Mahler, M. Mapes, T. Miller, G. Narayan, M. Paniccia, T. Roser, F. Severino, J. Skaritka, L. Smart, K. Smith, V. Soria, Y. Than, J. Tuozzolo, E. Wang, B. Xiao, T. Xin, I. Ben-Zvi, C. Boulware, T. Grimm, K. Mihara, D. Kayran, and T. Rao, *Phys. Rev. Lett.* **124**, 244801 (2020).
- [14] H. Chaloupka, H. Heinrichs, A. Michalke, H. Piel, C. Sinclair, F. Ebeling, T. Weiland, U. Klein, and H. Vogel, *Nucl. Instrum. Methods Phys. Res., Sect. A* **285**, 327 (1989).
- [15] R. Calaga, I. Ben-Zvi, M. Blaskiewicz, X. Chang, D. Kayran, and V. Litvinenko, *Physica C: Superconductivity* **441**, 159 (2006).
- [16] J. R. Harris, K. L. Ferguson, J. W. Lewellen, S. P. Niles, B. Rusnak, R. L. Swent, W. B. Colson, T. I. Smith, C. H. Boulware, T. L. Grimm, P. R. Cunningham, M. S. Curtin, D. C. Miccolis, D. J. Sox, and W. S. Graves, *Phys. Rev. ST Accel. Beams* **14**, 053501 (2011).
- [17] J. Teichert, A. Arnold, G. Ciovati, J.-C. Deinert, P. Evtushenko, M. Justus, J. M. Klopff, P. Kneisel, S. Kovalev, M. Kuntzsch, U. Lehnert, P. Lu, S. Ma, P. Murcek, P. Michel, A. Ryzhov, J. Schaber, C. Schneider, R. Schurig, R. Steinbrück, H. Vennekate, I. Will, and R. Xiang, *Phys. Rev. Accel. Beams* **24**, 033401 (2021).
- [18] B. Carlsten, *Nucl. Instrum. Methods Phys. Res., Sect. A* **285**, 313 (1989).
- [19] L. Serafini and J. B. Rosenzweig, *Phys. Rev. E* **55**, 7565 (1997).
- [20] M. Ferrario, D. Alesini, A. Bacci, M. Bellaveglia, R. Boni, M. Boscolo, M. Castellano, L. Catani, E. Chiadroni,

- S. Cialdi, A. Cianchi, A. Clozza, L. Cultrera, G. Di Pirro, A. Drago, A. Esposito, L. Ficcadenti, D. Filippetto, V. Fusco, A. Gallo, G. Gatti, A. Ghigo, L. Giannessi, C. Ligi, M. Mattioli, M. Migliorati, A. Mostacci, P. Musumeci, E. Pace, L. Palumbo, L. Pellegrino, M. Petrarca, M. Quattromini, R. Ricci, C. Ronsivalle, J. Rosenzweig, A. R. Rossi, C. Sanelli, L. Serafini, M. Serio, F. Sgamma, B. Spataro, F. Tazzioli, S. Tomassini, C. Vaccarezza, M. Vescovi, and C. Vicario, *Phys. Rev. Lett.* **99**, 234801 (2007).
- [21] D. H. Dowell, F. Zhou, and J. Schmerge, *Phys. Rev. Accel. Beams* **21**, 010101 (2018).
- [22] M. Gordon, W. H. Li, M. B. Andorf, A. C. Bartnik, C. J. R. Duncan, M. Kaemingk, C. A. Pennington, I. V. Bazarov, Y.-K. Kim, and J. M. Maxson, *Phys. Rev. Accel. Beams* **25**, 084001 (2022).
- [23] K. Zhao, J. Hao, Y. Hu, B. Zhang, S. Quan, J. Chen, and J. Zhuang, *Nucl. Instrum. Methods Phys. Res., Sect. A* **475**, 564 (2001).
- [24] R. Xiang, Y. Ding, K. Zhao, X. Lu, S. Quan, B. Zhang, L. Wang, S. Huang, L. Lin, and J. Chen, *Nucl. Instrum. Methods Phys. Res., Sect. A* **528**, 321 (2004).
- [25] J. Hao, X. Lu, Y. Ding, S. Quan, S. Huang, K. Zhao, B. Zhang, L. Wang, L. Lin, F. Jiao, G. Wang, D. Xie, F. Zhu, B. Xiao, R. Xiang, and J. Chen, *Nucl. Instrum. Methods Phys. Res., Sect. A* **557**, 138 (2006), energy Recovering Linacs 2005.
- [26] S. Quan, J. Hao, L. Lin, F. Zhu, F. Wang, L. Feng, S. Huang, Z. Wang, X. Wen, P. Fan, H. Xie, K. Liu, K. Zhao, and J. Chen, *Nucl. Instrum. Methods Phys. Res., Sect. A* **798**, 117 (2015).
- [27] S. Huang, K. Liu, K. Zhao, and J. Chen, *Chinese Science Bulletin* **68**, 1036 (2023).
- [28] D. Ouyang, Y. Zhao, H. Xie, X. Zhang, S. Zhao, L. Feng, K. Liu, and S. Huang, *Nucl. Instrum. Methods Phys. Res., Sect. A* **1026**, 166204 (2022).
- [29] T. Wang, H. Xu, Z. Liu, X. Zhang, J. Liu, J. Xu, L. Feng, J. Li, K. Liu, and S. Huang, *Opt. Express* **32**, 9699 (2024).
- [30] R. Xiang and J. Teichert, *Physics Procedia* **77**, 58 (2015), international Conference on Laser Applications at Accelerators, LA3NET 2015, 25-27 March 2015, Mallorca, Spain.
- [31] E. Wang, V. N. Litvinenko, I. Pinayev, M. Gaowei, J. Skaritka, S. Belomestnykh, I. Ben-Zvi, J. C. Brutus, Y. Jing, J. Biswas, J. Ma, G. Narayan, I. Petrushina, O. Rahman, T. Xin, T. Rao, F. Severino, K. Shih, K. Smith, G. Wang, and Y. Wu, *Scientific Reports* **11**, 4477 (2021).
- [32] F. Zhou, C. Adolphsen, A. Benwell, G. Brown, D. H. Dowell, M. Dunning, S. Gilevich, K. Grouev, G. Huang, B. Jacobson, X. H. Liu, A. Miahnahri, F. Sannibale, J. Schmerge, and T. Vecchione, *Phys. Rev. Accel. Beams* **24**, 073401 (2021).
- [33] T. Tan, H. Jia, S. Zhao, T. Li, T. Wang, Z. Liu, X. Zhang, S. Huang, L. Lin, L. Feng, H. Xie, S. Quan, and K. Liu, *Nucl. Instrum. Methods Phys. Res., Sect. A* **1045**, 167552 (2023).
- [34] S. Zhao, S. Huang, L. Lin, Y. Liu, H. Jia, W. Qin, S. Quan, and K. Liu, *Nucl. Instrum. Methods Phys. Res., Sect. A* **1018**, 165796 (2021).
- [35] I. V. Bazarov, B. M. Dunham, and C. K. Sinclair, *Phys. Rev. Lett.* **102**, 104801 (2009).